ARTICLE IN PRESS

ELSEVIER

Chemical Geology 14156 (2003) 1–23

CHEMICAL GEOLOGY
INCLUDING
ISOTOPE GEOSCIENCE

www.elsevier.com/locate/chemgeo

Osmium isotopic constraints on the age of lithospheric mantle beneath northeastern China

Fu-yuan Wu[a,*], Richard J. Walker[b], Xiang-wen Ren[a], De-you Sun[a], Xin-hua Zhou[c]

[a] *Department of Geology, Jilin University, 79 Jianshejie, 130061 Changchun, China*
[b] *Isotope Geochemistry Laboratory, Department of Geology, University of Maryland, College Park, MD 20742, USA*
[c] *Institute of Geology and Geophysics, Chinese Academy of Sciences, Qijiahuozi, 100029 Beijing, China*

Abstract

Northeastern China is composed of the Paleozoic Xing'an Mongolian Orogenic Belt (XMOB) in the north, and the Archean North China Craton (NCC) in the south. Mantle xenoliths from the subcontinental lithospheric mantle (SCLM) underlying these crustal blocks were entrained in Cenozoic basalts and brought to the surface. The Os isotopic compositions of these xenoliths are quite variable. The most refractory xenoliths ($Al_2O_3 < 1.2$ wt.%) from both blocks yield model Os T_{RD} ages between 1.2 and 0.4 Ga. For the XMOB, this indicates that some portions of the underlying SCLM are approximately the same age as the overlying continental crust. This is typical of the age relations between SCLM and the overlying crust for most cratons. The refractory xenoliths with minimally depleted $^{187}Os/^{188}Os$, however, suggest the addition of much younger, Phanerozoic lithospheric mantle. The lack of any xenoliths with Archean model ages in the SCLM underlying the NCC, sampled by this study, suggests that the original SCLM underlying the NCC block has been largely removed. This may have occurred during the Proterozoic, the Phanerozoic, or during both periods. These results highlight the complex age structure in the current SCLM beneath northeastern China, with lithosphere ranging in age from Proterozoic to additions within the past several 100 Ma.

Keywords: Os isotopes; Crust–mantle decoupling; Lithospheric mantle; Northeastern China

1. Introduction

Recent studies of northeastern China have suggested that a significant portion of the original subcontinental lithospheric mantle (SCLM) underlying Archean and Proterozoic cratons were removed subsequent to the early Paleozoic. This conclusion is based on the occurrence of early Paleozoic diamondiferous kimberlites in Mengyin of Shandong (central eastern China) and Fuxian of Liaoning (northeastern China), both of which are located within the Archean North China Craton (NCC) (Fig. 1). The presence of these rocks implies the existence of thick (≈ 200 km), lithospheric mantle at the time of volcanism (Menzies et al., 1993; Griffin et al., 1998; Wang et al., 1998). Mantle xenoliths with Archean Os model ages from Fuxian provide strong evidence that at least some portions of the SCLM underlying the NCC were Archean at that time (Gao et al., 2002). Geophysical data and isotopic studies of mantle xenoliths taken

* Corresponding author. Tel.: +86-431-8502322; fax: +86-431-8502274.
E-mail addresses: wufuyuan@jlu.edu.cn (F. Wu), rjwalker@geol.umd.edu (R.J. Walker), zhouxh@public3.bta.net.cn (X. Zhou).

0009-2541/02/$ - see front matter © 2002 Elsevier Science B.V. All rights reserved.
doi:10.1016/S0009-2541(02)00409-6

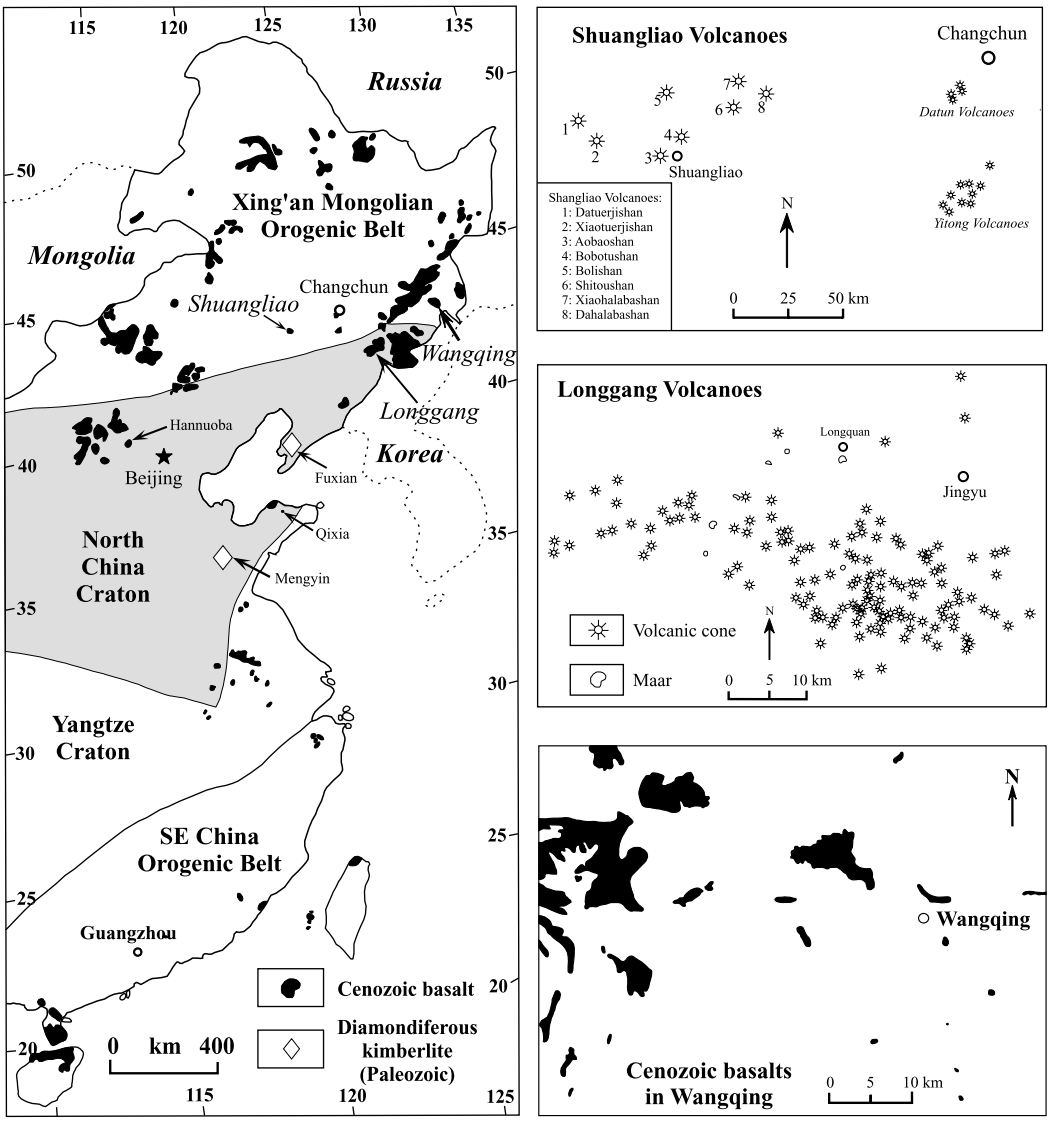

Fig. 1. Simplified distribution map of Cenozoic volcanic rocks in Eastern China. The samples of this study are from its northeastern part, which consists of Xing'an Mongolian Orogenic Belt (XMOB) in the north, and North China Craton (NCC) in the south. Paleozoic and Cenozoic volcanic rocks from which mantle xenoliths were sampled by Gao et al. (2002) are also shown for comparison (Fuxian, Hannuoba and Qixia).

from Cenozoic basalts, however, suggest that the present lithosphere is much thinner (60–120 km) (Menzies et al., 1993; Menzies and Xu, 1998; Griffin et al., 1998; Fan et al., 2000; Xu et al., 2000; Gao et al., 2002). For example, Gao et al. (2002) reported Proterozoic through Phanerozoic Os model melt extraction ages for refractory mantle xenoliths from two Tertiary volcanic centers, Qixia and Hannuoba. This suggests that a portion of the ancient SCLM that once underlay northeastern China was replaced with thinner, most likely younger lithosphere, subsequent to the early Paleozoic.

Our objective here is to expand the areal sampling of SCLM xenoliths in northeastern China and further examine the age structure of the SCLM underlying that region. Towards that end, we have

analyzed mantle xenoliths from Longgang, located in the northeastern portion of the NCC, and also samples from Shungliao and Wangqing, locations within the Phanerozoic Xing'an Mongolian Orogenic Belt (XMOB) which adjoins the northern boundary of the NCC.

2. Geological background

Northeastern China is divided into two major tectonic units, the XMOB in the north, and the NCC in the south (Fig. 1). The XMOB is the eastern part of the Paleozoic Central Asian Orogenic Belt (CAOB), located between the Siberian craton and the NCC (Jahn et al., 2000). The XMOB is primarily constructed of granites, characterized by low initial Sr ratios, positive $\varepsilon_{Nd}(t)$ values and relatively young T_{DM} Nd model ages (0.5–1.0 Ga) (Jahn et al., 2000). The average T_{DM} Nd isotopic model age of these granitic rocks is 0.89 ± 0.22 Ga (Fig. 2).

The NCC is the oldest tectonic unit in China, containing crust as old as 3800 Ma (Liu et al., 1992). It is characterized by widespread distribution of a late Archean tonalite–trondhjemite–granite suite with minor amounts of supracrustal rocks. A Paleo- to Mesoproterozoic rift basin developed in the southern part of this craton. It has been suggested that the craton was stabilized during the Paleoproterozoic and subsequently covered by a thick sequence of Proterozoic to Paleozoic sediments. A sedimentary gap developed during the middle Paleozoic (O_1–C_2). The Nd T_{DM} model ages of the felsic rocks in this craton are Archean and range mainly between 2.5 and 2.9 Ga, but with two peaks at 2.6–2.8 and 3.2–3.6 Ga (Wu et al., 1997) (Fig. 2).

Since the late Mesozoic, northeastern China became an important part of the circum-Pacific tectonic–magmatic zone. During this stage (Yanshanian Period), intensive deformation, mineralization, and igneous activity occurred (Wang and Mo, 1996), including extensive eruption of intermediate-acid volcanic rocks and wide-scale emplacement of granites.

During the Cenozoic, extensive eruption of basalts occurred. Some of these basalts contain ultramafic

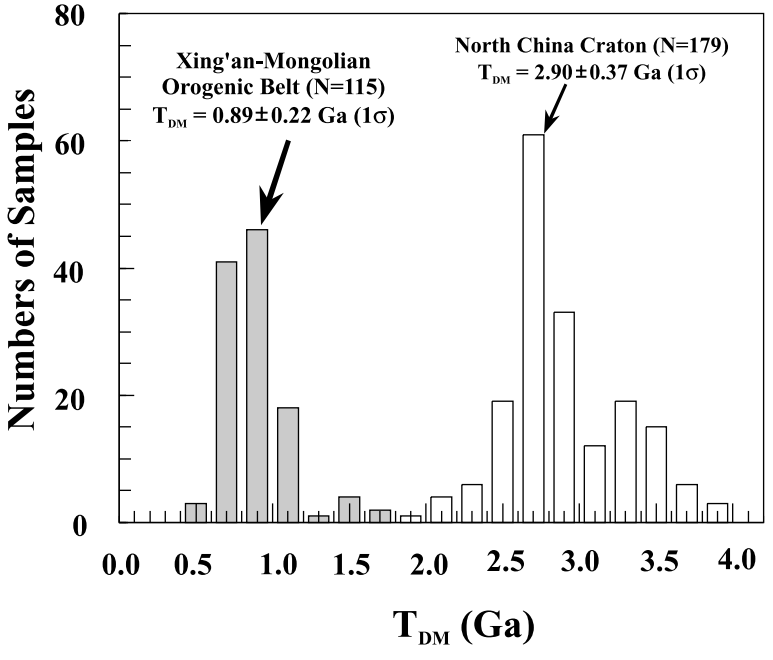

Fig. 2. Nd T_{DM} isotopic model age distributions of felsic rocks in the NCC and XMOB (Wu et al., 2000, 2002, 2003). The results show that these two tectonic units have very different crust formational ages.

Table 1
Chemical compositions of mantle peridotites in Longgang, NE China

Sample	DYS1-01	DYS1-03	DYS1-05	LQL1-01	LQL1-01(R)	LQL1-02	LQL1-02(R)	LQL1-13	L-1	L-2	L-2(R)	L-5	DAL2-02	DAL2-03	DAL2-03(R)
Major elements (wt.%)															
SiO_2	43.64	41.42	42.44	42.70		43.39		42.59	43.65	43.93		44.73	42.51	40.65	
TiO_2	0.09	0.04	0.07	0.02		0.07		0.03	0.09	0.13		0.15	0.02	0.02	
Al_2O_3	3.33	0.81	1.22	1.12		2.53		1.54	1.75	3.15		3.23	0.64	0.41	
TFe_2O_3	8.30	8.93	9.38	9.38		9.08		8.57	8.99	9.33		8.93	9.10	9.97	
MnO	0.12	0.12	0.17	0.18		0.16		0.14	0.16	0.15		0.15	0.13	0.12	
MgO	39.96	46.27	44.74	44.30		41.20		44.27	43.77	40.42		39.57	45.11	48.55	
CaO	3.18	1.28	0.66	0.94		2.30		1.51	1.30	2.64		3.08	2.64	0.47	
Na_2O	0.19	0.04	0.04	0.08		0.14		0.04	0.18	0.30		0.22	0.40	0.06	
K_2O	0.01	0.01	0.01	0.01		0.01		0.01	< 0.01	< 0.01		< 0.01	0.01	0.01	
P_2O_5	0.02	0.02	0.01	0.02		0.01		0.01	0.01	0.01		0.01	0.02	0.02	
Ig(LOS)	− 0.34	− 0.49	− 0.44	− 0.41		− 0.43		− 0.27	− 0.52	− 0.42		− 0.45	− 0.64	− 0.76	
Total	98.5	98.45	98.3	98.34		98.46		98.44	99.38	99.64		99.62	99.94	99.52	
Trace elements (ppm)															
Li	2.06	2.20	1.80	2.71	2.73	1.99	2.44	2.17					2.84	2.41	2.45
Be	0.013	0.035	0.018	0.24	0.18	0.019	0.015	0.009	0.036	0.023	0.013	0.042	0.14	0.010	0.028
Sc	17.8	10.6	8.18	11.0	10.6	10.3	11.6	11.5	9.4	101	13.5	15.9	10.6	5.87	5.54
V	75.7	32.1	32.3	36.8	37.4	52.3	54.5	41.2	35.3	59.8	63.4	65.3	33.6	16.4	14.7
Cr	2898	2330	2626	2240	2227	2061	2138	2404	2798	2155	2312	2642	3045	1201	1179
Co	102	116	117	114	112	109	108	107	104	94.8	110	94	113	130	129
Ni	1725	2104	2064	2020	1940	1862	1838	1895	2088	1897	1798	1772	2053	2364	2365
Cu	7.88	3.99	2.39	4.13	5.39	3.11	2.72	4.51	7.18	7.59	8.33	7.79	2.80	7.18	7.32
Zn	41.8	39.0	44.5	38.7	39.0	38.6	39.2	37.3	48.5	44.9	50.2	64.2	42.2	38.5	39.5
Ga	2.91	1.01	1.41	1.04	1.09	1.97	2.10	1.17	2.10	2.73	2.63	2.67	0.95	0.62	0.60
Rb	0.12	0.15	0.097	0.087	0.14	0.063	0.062	0.048	0.186	4.32	0.052	0.310	0.066	0.037	0.039

Sr	5.00	8.30	1.29	2.08	3.65	2.04	2.16	3.93	8.36	4.97	5.93	10.15	61.2	3.38	3.30
Ba	2.23	2.76	1.13	14.0	14.7	7.84	7.99	0.65	5.10	0.52	8.46	9.10	7.17	1.04	0.94
Y	3.45	1.08	0.58	0.33	0.47	1.87	1.89	0.67	2.50	1.10	3.12	3.45	3.36	0.44	0.42
Zr	2.68	7.21	3.35	0.63	1.46	1.88	1.98	0.81	10.69	2.80	2.27	3.93	19.2	0.49	0.46
Hf	0.12	0.15	0.091	0.014	0.030	0.070	0.072	0.019	0.406	0.108	0.13	0.15	0.15	0.017	0.016
Nb	0.086	0.27	0.079	0.13	0.22	0.12	0.11	0.096	0.073	0.13	0.064	0.100	2.40	0.054	0.043
Ta	0.006	0.020	0.004	0.007	0.011	0.005	0.006	0.006	0.005	0.019		0.04	0.13	0.004	0.004
Cs	0.004	0.005	0.005	0.004	0.004	0.002	0.002	0.001	0.009	0.008	0.005	0.006	0.004	0.001	0.001
Pb	0.69	0.48	28.1	0.65	0.64	0.21	0.27	0.21	0.81	0.34	0.74	1.01	0.37	0.24	0.25
Th	0.006	0.042	0.008	0.40	0.39	0.011	0.012	0.010	0.059	0.038	0.045	0.011	0.054	0.023	0.022
U	0.004	0.010	0.005	0.12	0.11	0.010	0.010	0.010	0.024	0.035	0.046	0.014	0.016	0.014	0.014
Rare earth elements (ppm)															
La	0.12	0.45	0.059	0.40	0.47	0.27	0.26	0.12	0.31	0.125	0.33	0.16	1.15	0.16	0.16
Ce	0.34	0.94	0.13	0.51	0.67	0.31	0.33	0.25	0.46	0.242	0.43	0.42	4.11	0.28	0.27
Pr	0.072	0.12	0.019	0.059	0.082	0.075	0.075	0.034	0.057	0.032	0.073	0.092	0.70	0.033	0.030
Nd	0.49	0.61	0.12	0.23	0.33	0.36	0.37	0.16	0.40	0.190	0.44	0.56	3.50	0.14	0.13
Sm	0.23	0.17	0.066	0.045	0.064	0.13	0.13	0.042	0.213	0.089	0.18	0.24	0.91	0.046	0.038
Eu	0.083	0.056	0.025	0.014	0.019	0.046	0.048	0.015	0.084	0.035	0.077	0.095	0.28	0.017	0.014
Gd	0.27	0.16	0.075	0.045	0.067	0.15	0.15	0.050	0.263	0.119	0.27	0.29	0.76	0.048	0.047
Tb	0.069	0.030	0.016	0.007	0.011	0.037	0.035	0.011	0.058	0.025	0.057	0.067	0.13	0.011	0.010
Dy	0.49	0.18	0.097	0.040	0.061	0.26	0.26	0.075	0.397	0.197	0.45	0.49	0.66	0.066	0.065
Ho	0.12	0.037	0.022	0.010	0.014	0.063	0.063	0.022	0.086	0.047	0.098	0.110	0.13	0.016	0.016
Er	0.31	0.089	0.053	0.029	0.035	0.17	0.17	0.057	0.227	0.137	0.31	0.31	0.27	0.040	0.038
Tm	0.053	0.013	0.009	0.006	0.007	0.027	0.028	0.011	0.038	0.022	0.056	0.053	0.041	0.006	0.006
Yb	0.38	0.098	0.060	0.051	0.062	0.20	0.21	0.084	0.236	0.146	0.34	0.36	0.27	0.051	0.045
Lu	0.060	0.016	0.010	0.009	0.011	0.033	0.034	0.014	0.034	0.024	0.055	0.056	0.039	0.008	0.008

Table 2
Chemical compositions of mantle peridotites in Shuangliao, NE China

Sample	ABS1-5	ABS1-5(R)	ABS2-21	BBT1-2	BBT1-2(R)	BBT1-2(R)	BBT1-8	BBT1-8(R)	BBT1-12	BBT1-14	BBT2-12	BLS1-8	BLS1-8(R)	BLS1-9	BLS1-9(R)	BL1-10	BL1-12
Major elements (wt.%)																	
SiO_2	43.50		44.67	43.24			41.80		43.15	43.90	44.43	44.25		43.22		44.92	44.03
TiO_2	0.06		0.10	0.10			0.25		0.07	0.02	0.05	0.08		0.11		0.08	0.07
Al_2O_3	1.58		2.97	2.67			2.45		1.51	1.10	1.20	1.79		2.26		3.09	3.05
TFe_2O_3	9.16		8.48	8.76			12.81		9.31	8.96	8.08	8.70		9.32		7.96	8.78
MnO	0.17		0.12	0.15			0.20		0.14	0.16	0.13	0.16		0.17		0.13	0.13
MgO	43.99		39.93	41.19			37.71		40.72	41.02	42.42	43.81		42.01		40.21	39.64
CaO	1.38		3.12	2.09			2.02		3.31	3.29	1.85	1.33		1.99		3.12	3.46
Na_2O	0.10		0.17	0.19			1.41		0.06	0.09	0.04	0.11		0.50		0.20	0.19
K_2O	0.16		0.04	0.04			0.11		0.05	0.01	0.02	<0.01		0.01		0.01	0.02
P_2O_5	0.07		0.02	0.01			0.03		0.02	0.02	0.02	0.01		0.01		0.02	0.01
Ig(LOS)	0.36		0.40	1.23			1.21		1.64	1.69	1.74	0.01		0.03		0.13	0.66
Total	100.53		100.02	99.67			100.00		99.98	100.26	99.98	100.25		99.63		99.87	100
Trace elements (ppm)																	
Li									5.51	4.14	6.23					3.43	2.70
Be	0.165	0.16	0.023	0.040	0.026	0.076	0.067	0.047	0.021	0.028	0.035	0.041	0.025	0.025	0.052	0.017	
Sc	7.38	5.83	12.8	12.1	13.4	9.14	8.25	10.0	11.3	9.87	10.0	9.08	14.0	11.8	14.5	12.6	
V	33.5	33.8	51.8	46.6	52.3	52.7	53.1	47.3	43.4	46.0	40.4	44.5	46.9	53.1	69.9	71.8	
Cr	2184	2173	2362	2115	2450	2177	2011	2406	3067	2733	2575	2670	2205	2503	3296	2669	
Co	97.2	112	101	90.0	107	99.7	107	106	104	99.5	98.1	116	93.8	114	97.2	102	
Ni	2108	1901	2115	1878	1807	1639	1470	1831	1855	1825	2143	1974	1974	1937	1629	1662	
Cu	11.6	11.2	18.0	16.1	16.4	17.5	16.8	10.1	13.5	14.8	17.3	16.7	13.7	13.7	6.03	22.6	
Zn	47.7	43.7	47.5	43.7	39.8	89.8	82.6	42.9	38.9	35.6	41.8	48.6	46.8	48.8	41.3	43.5	
Ga	1.69	1.85	2.18	1.94	2.07	4.09	3.68	1.54	1.07	1.07	1.53	1.67	2.05	2.15	2.80	2.72	
Rb	3.10	3.18	2.12	2.48	1.63	3.74	2.78	2.20	0.52	2.16	0.70	0.27	0.60	0.18	0.24	0.39	

Sr	62.6	64.0	23.5	24.0	20.4	41.4	33.8	76.8	127	27.2	11.8	12.6	11.2	11.7	6.86	36.7
Ba	14.1	18.9	5.46	5.02	49.9	8.05	16.0	2.12	1.75	1.02	3.34	2.68	0.92	6.16	0.56	1.28
Y	1.72	1.81	2.57	2.42	2.55	2.63	2.74	0.93	0.40	0.89	1.36	1.38	1.91	2.04	2.86	2.55
Zr	6.60	6.01	3.64	3.42	3.38	9.49	9.35	2.51	2.42	2.62	8.86	8.52	6.18	6.05	11.0	1.18
Hf	0.091	0.12	0.098	0.082	0.10	0.280	0.30	0.043	0.041	0.070	0.106	0.11	0.124	0.17	0.19	0.069
Nb	2.80	2.68	0.55	0.49	0.53	0.87	0.86	0.39	0.16	0.34	0.48	0.46	0.45	0.42	0.95	0.047
Ta	0.117	0.099	0.034	0.031	0.011	0.074	0.045	0.036	0.019	0.022	0.037	0.016	0.030	low	0.006	0.003
Cs	0.013	0.015	0.010	0.015	0.013	0.015	0.020	0.005	0.002	0.005	0.016	0.020	0.018	0.017	0.009	0.010
Pb	0.56	0.91	0.21	0.25	4.17	0.44	1.50	0.23	0.41	0.29	0.37	2.06	0.93	1.26	0.25	0.30
Th	0.47	0.37	0.06	0.07	0.039	0.16	0.095	0.048	0.043	0.048	0.09	0.041	0.03	0.028	0.000	<0.001
U	0.14	0.16	0.02	0.02	0.026	0.05	0.021	0.018	0.011	0.015	0.03	0.041	0.02	0.023	0.024	0.001
Rare earth elements (ppm)																
La	4.459	5.30	0.354	0.403	0.41	1.276	1.35	0.52	0.45	0.31	0.807	0.71	0.360	0.44	0.088	0.020
Ce	9.177	10.2	0.919	0.955	0.89	3.572	3.46	1.09	0.91	0.68	1.723	1.43	1.056	1.18	0.34	0.076
Pr	0.870	1.12	0.105	0.116	0.12	0.454	0.49	0.13	0.11	0.095	0.181	0.18	0.127	0.16	0.07	0.021
Nd	3.121	3.94	0.518	0.563	0.55	2.162	2.20	0.54	0.41	0.45	0.663	0.63	0.717	0.78	0.45	0.21
Sm	0.509	0.58	0.132	0.148	0.14	0.539	0.52	0.11	0.074	0.13	0.141	0.14	0.167	0.22	0.19	0.13
Eu	0.140	0.16	0.053	0.047	0.082	0.152	0.17	0.030	0.022	0.036	0.048	0.053	0.055	0.077	0.07	0.052
Gd	0.430	0.57	0.223	0.214	0.26	0.436	0.52	0.106	0.069	0.13	0.155	0.20	0.197	0.23	0.25	0.19
Tb	0.062	0.075	0.050	0.048	0.047	0.089	0.086	0.019	0.011	0.023	0.029	0.030	0.042	0.045	0.060	0.045
Dy	0.337	0.35	0.358	0.355	0.33	0.509	0.46	0.13	0.064	0.15	0.196	0.20	0.296	0.33	0.38	0.35
Ho	0.057	0.060	0.084	0.083	0.077	0.094	0.086	0.030	0.013	0.032	0.047	0.045	0.066	0.075	0.10	0.091
Er	0.147	0.16	0.246	0.233	0.26	0.237	0.22	0.088	0.033	0.072	0.132	0.14	0.171	0.20	0.26	0.23
Tm	0.022	0.031	0.041	0.040	0.047	0.036	0.038	0.015	0.007	0.012	0.023	0.028	0.028	0.035	0.045	0.041
Yb	0.124	0.16	0.256	0.222	0.30	0.202	0.21	0.12	0.052	0.082	0.145	0.17	0.186	0.25	0.30	0.29
Lu	0.020	0.026	0.048	0.044	0.057	0.031	0.033	0.019	0.009	0.014	0.022	0.026	0.028	0.044	0.049	0.047

Table 3
Chemical compositions of mantle peridotites in Wangqing, NE China

Sample	WQ00-6	WQ00-12	WQ00-13	WQ00-17	WQ00-18	WQ00-19	WQ00-26	WQ00-26(R)
Major elements (wt.%)								
SiO_2	44.26	42.34	43.72	44.78	44.15	44.78	44.72	44.68
TiO_2	0.12	0.02	0.02	0.10	0.10	0.14	0.03	0.03
Al_2O_3	3.20	0.38	1.07	2.69	1.72	4.02	1.81	1.82
TFe_2O_3	9.20	9.08	9.35	9.57	10.01	9.31	9.32	9.30
MnO	0.13	0.12	0.12	0.13	0.13	0.13	0.13	0.12
MgO	39.95	47.55	45.00	40.60	43.04	38.69	42.65	42.50
CaO	2.84	0.53	1.08	2.26	1.50	2.70	1.52	1.52
Na_2O	0.24	0.07	0.09	0.18	0.17	0.27	0.11	0.11
K_2O	0.09	0.04	0.04	0.02	0.04	0.03	0.01	0.01
P_2O_5	0.01	0.03	0.01	0.01	0.02	0.01	0.01	0.01
Ig(LOS)	− 0.52	− 0.45	− 0.50	− 0.56	− 0.62	− 0.58	− 0.55	− 0.55
Total	99.52	99.71	100.00	99.78	100.26	99.50	99.76	99.55
Trace elements (ppm)								
Li	4.75	4.39	3.14	2.73	3.05	2.97	1.85	1.99
Be	0.079	0.052	0.039	0.060	0.043	0.014	0.024	0.026
Sc	16.0	4.84	11.7	15.0	10.1	10.7	12.8	12.6
V	74.3	13.8	39.9	68.9	46.0	79.1	50.7	50.3
Cr	2485	1957	2118	2582	2275	2648	2497	2431
Co	106	121	113	104	109	105	110	109
Ni	1739	2249	1857	1737	1687	1687	1826	1797
Cu	14.8	2.25	5.91	16.3	19.1	18.2	9.04	8.55
Zn	45.2	37.3	37.7	47.2	47.7	47.7	36.6	35.2
Ga	2.82	0.72	1.07	2.48	2.03	3.53	1.61	1.48
Ge	1.03	0.85	0.91	1.03	0.86	0.97	0.95	0.83
Rb	1.25	0.77	0.72	0.24	0.61	0.32	0.46	0.46
Sr	12.6	13.3	11.7	9.56	15.1	7.11	4.09	3.85
Ba	2.93	3.48	2.32	1.87	5.03	1.20	0.95	0.88
Y	3.54	3.23	0.93	2.15	1.93	3.32	0.96	0.92
Zr	4.58	1.55	3.24	3.66	8.45	4.71	1.49	1.42
Hf	0.14	0.028	0.067	0.098	0.21	0.16	0.029	0.032
Nb	0.22	0.43	0.23	0.35	0.84	0.072	0.14	0.12
Ta	0.008	0.015	0.008	0.027	0.065	0.005	0.008	0.006
Sn	0.083	0.085	0.060	0.075	0.093	0.088	0.043	0.045
Cs	0.011	0.012	0.015	0.006	0.021	0.007	0.029	0.026
Pb	0.76	0.38	0.40	0.51	0.72	0.54	0.40	0.38
Th	0.27	0.65	0.19	0.073	0.16	0.003	0.027	0.026
U	0.065	0.11	0.046	0.023	0.040	0.028	0.015	0.016
Rare earth elements (ppm)								
La	2.13	8.91	1.72	0.56	1.29	0.10	0.18	0.16
Ce	3.47	14.5	2.99	1.20	2.85	0.42	0.37	0.34
Pr	0.36	1.44	0.32	0.15	0.36	0.089	0.056	0.053
Nd	1.29	4.66	1.20	0.72	1.52	0.55	0.27	0.25
Sm	0.32	0.71	0.21	0.19	0.34	0.23	0.077	0.067
Eu	0.10	0.16	0.049	0.064	0.095	0.084	0.027	0.022
Gd	0.38	0.73	0.19	0.21	0.31	0.28	0.081	0.070
Tb	0.074	0.097	0.028	0.045	0.056	0.069	0.018	0.017
Dy	0.48	0.50	0.15	0.30	0.32	0.46	0.12	0.12
Ho	0.12	0.10	0.033	0.075	0.066	0.11	0.033	0.032
Er	0.31	0.26	0.085	0.20	0.18	0.29	0.093	0.090

Table 3 (*continued*)

Sample	WQ00-6	WQ00-12	WQ00-13	WQ00-17	WQ00-18	WQ00-19	WQ00-26	WQ00-26(R)
Rare earth elements (ppm)								
Tm	0.051	0.043	0.014	0.034	0.029	0.051	0.017	0.017
Yb	0.35	0.30	0.11	0.24	0.19	0.36	0.13	0.12
Lu	0.057	0.048	0.018	0.040	0.031	0.056	0.021	0.021

xenoliths (Zhou et al., 1988; Fan and Hooper, 1989; Liu, 1992). Numerous studies have been conducted on these rocks (e.g. Zhou and Armstrong, 1982; E and Zhao, 1987; Chi, 1988; Peng et al., 1986; Basu et al., 1991; Liu, 1992; Tatsumoto et al., 1992; Xu et al., 1993, 1998, 2000, in press; Qi et al., 1995; Zhang et al., 1995, 2000; Snyder et al., 1997; Zheng et al., 1998, 2001; Fan et al., 2000). The basaltic rocks have been grouped into three successive episodes: (1) late Cretaceous–Paleogene subalkalic and alkalic basalts; (2) Neogene alkalic basalts with minor amounts of tholeiitic basalt, and (3) Quaternary alkalic basalts with subsidiary tholeiitic basalt (Fan and Hooper, 1989; Liu, 1992). These basalts indicate an alkali-rich trend during the progression of Cenozoic basaltic magmatism. The ultramafic xenoliths are mostly found in the Neogene and Quaternary alkaline basalts, and are generally not found in the tholeiitic flows, or in the late Cretaceous–Paleogene basalts (Fan and Hooper, 1989).

3. Sample descriptions

The xenoliths studied here come from three localities within these two tectonic domains: the Longgang volcanic field within the NCC, and the Shuangliao and Wangqing volcanic fields in the XMOB (Fig. 1). The Longgang volcanic field, located in the northeastern part of the NCC, contains more than 160 Quaternary volcanoes and maars, with the youngest eruption taking place only about 1600 years B.P. Samples were collected from the Longquan Maar, and the Dayishan and Dalongwan volcanoes, whose eruption ages are about 1.2 Ma, according to K/Ar dating of an adjacent maar (Liu, 1999). Mantle xenoliths are widely distributed with diameters ranging mostly between 5 and 10 cm. Spinel lherzolite is the most common rock type in this area with minor amounts of spinel harzburgite and pyroxenite, as at other basaltic localities in Eastern China and worldwide (Fan and Hooper, 1989). The xenoliths are mostly coarse-grained and equigranular, but porphyritic textures are present in some. No strongly foliated types have been found. The rocks are fresh and do not contain secondary alteration minerals. Primary minerals are clinopyroxene (3–20%), orthopyroxene (20–25%), olivine (50–70%) and spinel (3–5%). It should be noted that one sample (DYS1-05) contains hornblende indicating modification via aqueous-rich metasomatism (Downes, 2001).

The Shuangliao volcanic field of the XMOB, the oldest Cenozoic volcanoes in eastern China, consists of eight volcanoes: the Bobotushan, Aobaoshan, Bolishan, Dahalabashan, Xiaohalabashan, Datuerjishan, Xiaotuerjishan and Shitoushan (Fig. 1). The host volcanic rocks range from dolerites in Datuerjishan and Xiaotuerjishan, to alkaline olivine basalt in Dahalabashan, Xiaohalabashan and Shitushan, and basanite in Bobotushan, Aobaoshan and Bolishan (Yu, 1987; Liu, 1999). K–Ar ages for these rocks

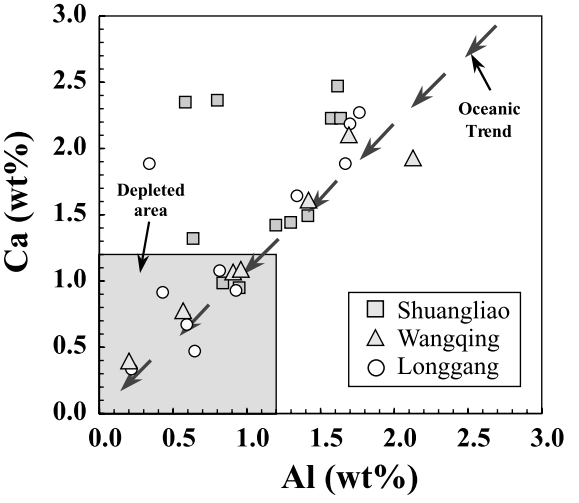

Fig. 3. Plots of Ca (wt.%) against Al (wt.%) for all xenoliths examined. The oceanic trend and depleted area are from Boyd (1989) and are shown for comparison.

Table 4
Rhenium–osmium isotopic and composition data for mantle xenoliths from NE China

Sample number	Location	t (Ma)	A_2O_3 (wt.%)	Fo (Olivine)	Cr# (Spinel)	T (°C)	Re (ppb)	Os (ppb)	$^{187}Re/^{188}Os$	$^{187}Os/^{188}Os$	γ_{Os}	T_{RD} (Ga)	T_{MA} (Ga)
Xing'an Mongolian Orogenic Belt													
ABS1-5	Aobaoshan, Shuangliao	40	1.58	91.14	26.69	964	0.418	4.948	0.406	0.12625	−0.6	0.11	−12.33
ABS2-21	Aobaoshan, Shuangliao	40	2.97	90.27	9.95	982	0.285	3.478	0.395	0.12680	−0.2	0.03	1.72
BLS1-8	Bolishan, Shuangliao	40	1.79	90.76	27.58	926	0.152	5.086	0.144	0.11813	−6.9	1.31	2.03
BLS1-9	Bolishan, Shuangliao	40	2.26	90.53	43.69	1152	0.086	0.447	0.926	0.12523	−1.7	0.26	−0.20
BL1-10	Bolishan, Shuangliao	40	3.09	90.98	14.04	968	0.066	1.920	0.165	0.12253	−3.4	0.66	1.12
BL1-12	Bolishan, Shuangliao	40	3.05	89.93	10.27	963	0.301	3.401	0.426	0.12889	1.5	−0.28	4.52
BBT1-2	Bobotushan, Shuangliao	40	2.67	90.79	13.46	1149	0.212	3.741	0.273	0.12125	−4.5	0.85	2.62
BBT1-8	Bobotushan, Shuangliao	40	2.45	90.10	19.81	856	0.073	2.556	0.138	0.11875	−6.4	1.22	1.85
BBT1-12	Bobotushan, Shuangliao	40	1.51	89.94	25.20	1131	0.335	3.368	0.479	0.12350	−2.8	0.52	−2.79
BBT1-14	Bobotushan, Shuangliao	40	1.10	90.83	44.84	1172	0.039	3.366	0.055	0.12344	−2.6	0.53	0.61
BBT2-12	Bobotushan, Shuangliao	40	1.20	91.07	42.47	1058	0.139	4.478	0.149	0.12216	−3.7	0.72	1.14
WQ00-6	Wangqing	3	3.20	89.69	10.72	1128	0.084	1.090	0.370	0.12710	0.1	−0.01	−0.19
WQ00-12	Wangqing	3	0.38	91.47	63.96	1194	0.003	1.587	0.010	0.12461	−1.9	0.36	0.36
WQ00-13	Wangqing	3	1.07	90.90	31.14	875	0.016	1.715	0.046	0.12272	−3.4	0.64	0.72
WQ00-17	Wangqing	3	2.69	89.82	13.38	941	0.090	1.105	0.394	0.12470	−1.8	0.34	15.41
WQ00-18	Wangqing	3	1.72	90.91	22.40	1106	0.084	1.919	0.209	0.11799	−7.1	1.33	2.74
WQ00-19	Wangqing	3	4.02	89.97	7.89	979	0.122	1.321	0.445	0.12689	−0.1	0.02	−0.15
WQ00-26	Wangqing	3	1.81	90.17	18.45	922	0.033	0.989	0.162	0.12561	−1.1	0.21	0.35
North China Craton (Longgang)													
L-1	Longquanlongwan	1.2	1.75	90.83	24.17	1119	<0.010	1.858	0.026	0.11916	−6.2	1.16	1.24
L-2	Longquanlongwan	1.2	3.15	89.77	11.44	1119	0.073	2.813	0.124	0.12561	−1.1	0.21	0.30
L-5	Longquanlongwan	1.2	3.23	90.15	12.60	1108	0.056	2.663	0.101	0.12677	−0.2	0.03	0.05
LQL1-01	Longquanlongwan	1.2	1.12	90.78	48.11	1040	0.014	2.838	0.024	0.12428	−2.1	0.40	0.43
LQL1-02	Longquanlongwan	1.2	2.53	90.02	11.65	910	0.017	0.864	0.092	0.12448	−2.0	0.38	0.49
LQL1-13	Longquanlongwan	1.2	1.54	91.23	23.94	1041	0.017	1.858	0.043	0.12011	−5.4	1.02	1.14
DYS1-01	Dayishan	1.2	3.33	90.37	9.96	971	0.064	2.307	0.134	0.12890	1.5	−0.28	−0.43
DYS1-03	Dayishan	1.2	0.81	91.03	39.35	1176	0.016	1.313	0.058	0.11876	−6.5	1.22	1.42
DYS1-05	Dayishan	1.2	1.22	90.60	33.85	975	0.015	0.112	0.625	0.12209	−3.9	0.73	−1.34
DAL02-2	Dalongwan	1.2	0.64	90.73	71.12		0.024	3.246	0.036	0.11860	−6.6	1.24	1.36
DAL02-3	Dalongwan	1.2	0.41	91.32	27.31	1197	0.075	1.119	0.322	0.12290	−3.2	0.61	3.00

All the reported values have been corrected for mass fractionation and blank (Re = 8 ± 2 pg, and Os = 3 ± 2 pg).
The parameters used in the calculation are $\lambda_{Re} = 1.666 \times 10^{-11}$/year, $(^{187}Re/^{188}Os)_{Chond} = 0.40186$ and $(^{187}Os/^{188}Os)_{Chond,0} = 0.1270$ (Shirey and Walker, 1998).
The volcanic eruption ages are from Liu (1999) and Xu et al. (1998).

range from 86 to 40 Ma, and display an increasing alkalinity with decreasing age. The ca. 40 Ma Bobotushan, Aobaoshan and Bolishan volcanoes contain most of the mantle xenoliths. The xenoliths are typically <10 cm in diameter, and are mainly spinel lherzolite, with minor spinel harzburgite and pyroxenite.

The Wangqing volcanic field, also of the XMOB, formed during the Miocene over an area of about 6 km^2. K–Ar ages range from 6.3 to 2.1 Ma (Liu, 1999). Spinel lherzolite is the most common xenolith type with minor spinel harzburgite and pyroxenite (E and Zhao, 1987; Fan and Hooper, 1989). The primary minerals of the peridotites are clinopyroxene (3–20%), orthopyroxene (20–25%), olivine (50–60%) and spinel (3–5%). The pyroxenite is composed of clinopyroxene and green spinel (<5%). The xenoliths are characterized by three different types of microstructures: protogranular, transitional and tabular equigranular (Xu et al., 1998). The rocks are fresh and do not contain secondary alteration minerals.

Using various geothermometers (Wu, unpublished and below), the equilibrium temperatures of samples from all three locales range from 840 to 1190 °C. It is difficult to assess the equilibrium pressures for the spinel peridotites, however, because they do not contain garnet. Studies of similar xenoliths from adjacent areas suggest that the samples examined here come from relatively shallow depths of 40–60 km (Xu et al., 1998). Temperature–pressure calculations, thus, suggest that the lithosphere underlying northeastern China during the Cenozoic was characterized by a high geothermal gradient, similar to that of southeastern Australia (E and Zhao, 1987; Xu et al., 2000).

4. Analytical techniques

Chemical analyses were conducted at the Department of Geology, Northwest University in Xi'an. Major elements were measured by X-Ray fluorescence method with analytical uncertainties ranging from 1% to 3%. Trace element concentrations (REE included) were determined using a POEMS III ICP-MS. The samples were dissolved in a two-step procedure to ensure refractory mineral dissolution. First, a mixture of $HF + HNO_3$ was added to each sample in a capped Teflon beaker and the beaker was placed on hot plate for evaporation. The solution was then dried, re-dissolved in $HF + HNO_3$, and the entire solution-residue assemblage was transferred into Teflon bombs with $HCl + HF + HNO_3$. The bomb dissolution lasted for 4 days at a temperature of ~140–190 °C. By then, no residue was detectable. The solutions were then transferred back into Teflon beakers and evaporated on a hot plate. The final precipitate was dis-

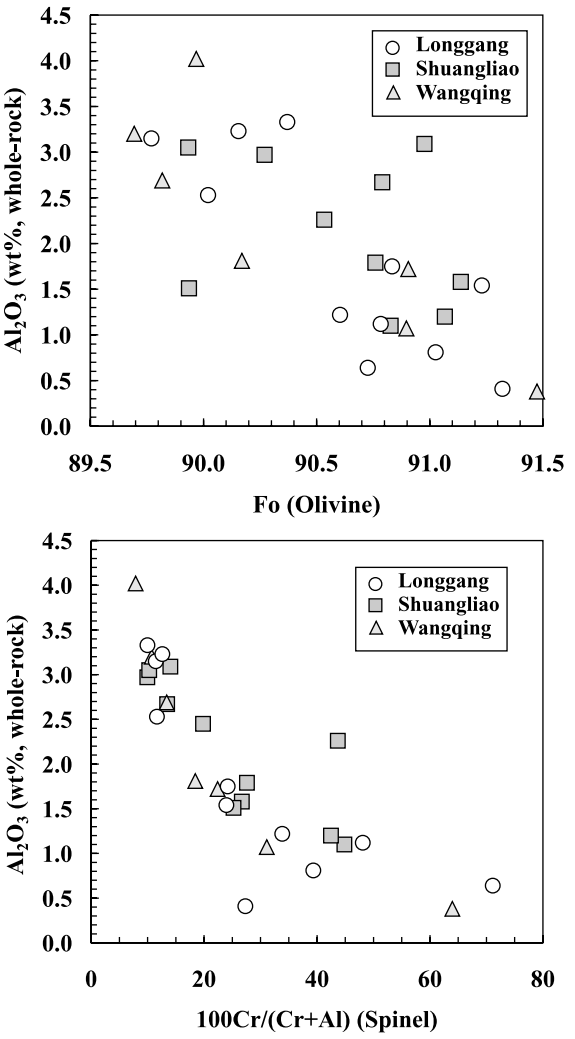

Fig. 4. Plots of Al_2O_3 (wt.%, whole-rock) versus Fo of olivine and Cr# (100Cr/(Cr + Al)) of spinel. The good correlations for samples from each locale suggest that the Al_2O_3 contents of most whole-rocks (see text) are viable indicators of fertility.

solved in dilute HNO_3 for ICP-MS analysis. The analytical precision for minor and trace elements is better than ± 10% (Hu et al., 2000).

The chemical-separation techniques used in this study for Re–Os analysis have been previously published (Shirey and Walker, 1995). Sample fragments devoid of weathering rind and host lava were processed first through a high-tensile strength alloy mortar and pestle and broken into cm-size chips. These chips were inspected for metal contamination and weathering surface prior to grinding into a fine powder with an agate shatter box. Whole-rock samples (3–4 g), spike of mixed ^{185}Re and ^{190}Os, and approximately 8 g of aqua regia were frozen into Carius tubes, sealed, and heated at 220–240 °C overnight to obtain sample-spike equilibration. In most cases, a silicate gel formed after 15 h of overnight at 220–240 °C. This gel prohibited the com-

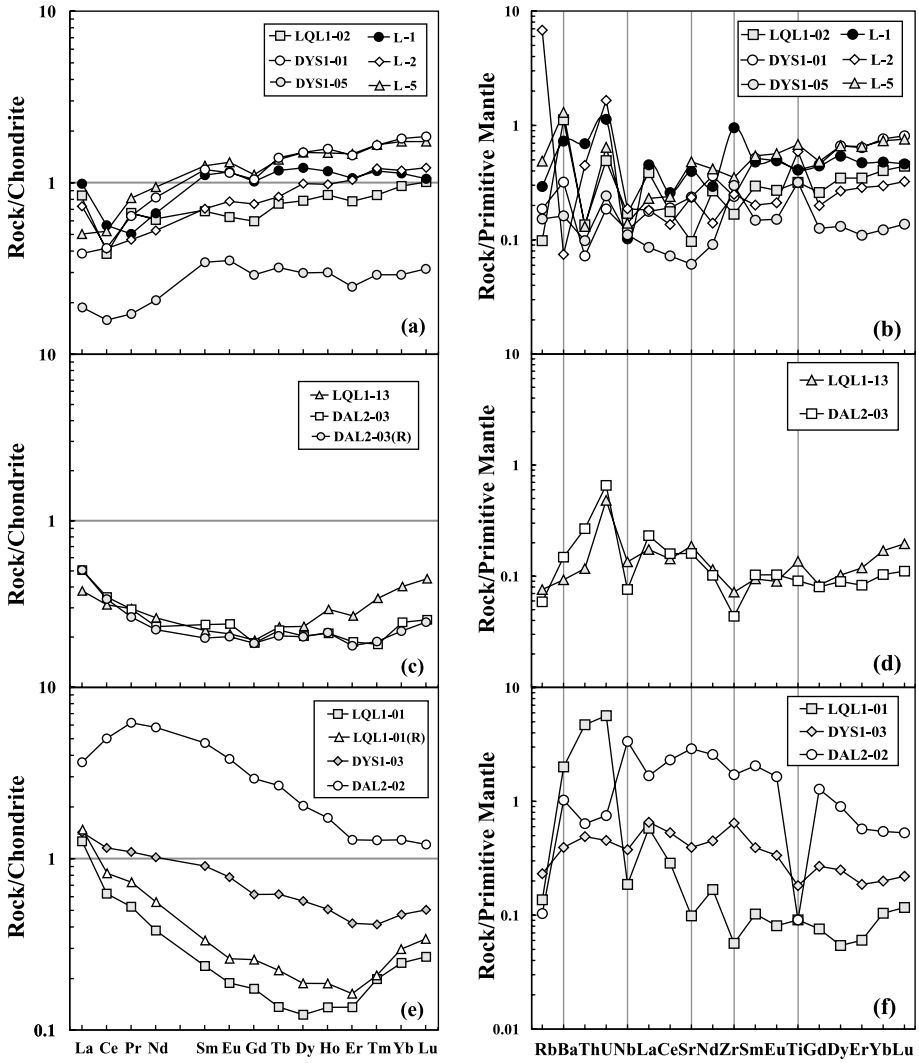

Fig. 5. Chondrite-normalized rare earth element patterns (a,c,e) and primitive mantle-normalized element patterns (b,d,f) for mantle peridotites from Longgang, NE China. The trace elements are arranged in the order of decreasing incompatibility from left to right. The normalized values are from Sun and McDonough (1989). The peridotites are divided into three groups based on REE pattern type.

plete attack (leach) of the remaining silicates, but did not affect the reproducibility of the Os concentration or $^{187}Os/^{188}Os$ ratio (Meisel et al., 2001). Most of the Os-bearing phases are presumed to be interstitial and effectively attacked by the acid mix. Osmium was purified using a carbon tetrachloride (CCl_4) solvent extraction technique (Cohen and Waters, 1996) follow by microdistillation purification. The Os total processing blank was 3 ± 2 pg and is inconsequential in all samples.

The remaining Carius tube liquid was dried and Re was separated and purified from this using two successive anion exchange columns (200–400 mesh) with resin volumes of 0.3 and 0.1 ml, respectively. The samples were loaded and eluted on columns using 0.1 N HNO_3, Re was then collected using 6 M HNO_3, and then dried under heat lamps (<80 °C). The Re blank for this procedure was 8 ± 2 pg.

Purified Re and Os were then loaded using $BaSO_4$ and $Ba(OH)_2$ as emission enhancers, respectively, on

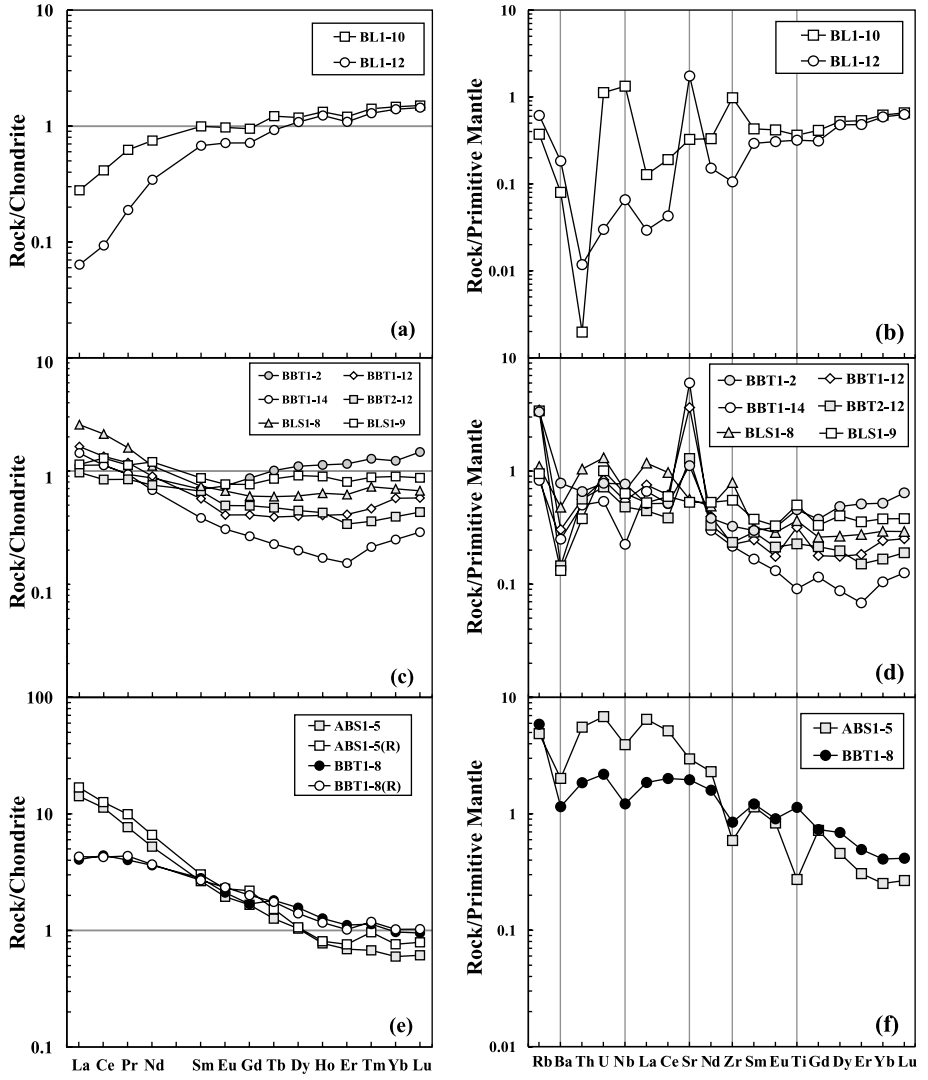

Fig. 6. Chondrite-normalized rare earth element patterns (a,c,e) and primitive mantle-normalized element patterns (b,d,f) for mantle peridotites from Shuangliao, NE China. The trace elements are arranged in the order of decreasing incompatibility from left to right. The normalized values are from Sun and McDonough (1989). The peridotites are divided into three groups based on REE pattern type.

platinum filaments and analyzed using negative thermal ionization mass spectrometry hosted at the University of Maryland, College Park. Mass spectrometric procedures have been discussed in Walker et al. (1994, 2002). Most of the analyses in this paper were conducted in a static mode using six Faraday cups on a *Sector 54* mass spectrometer. For these levels of Os (2–5 ng), external reproducibility in the $^{187}Os/^{188}Os$ ratio was about $\pm 0.1\%$ (2σ), based on repeated analyses of comparable quantities of a standard. Rhenium analyses were obtained using an NBS-12 inch mass spectrometer. In-run statistics were typically ± 0.1 to 0.3% (2σ). Repeated measurements of a Re standard suggest an external precision of approximate $\pm 0.3\%$ (2σ). Blank corrections limit absolute uncertainties for most samples to approximately $\pm 2\%$.

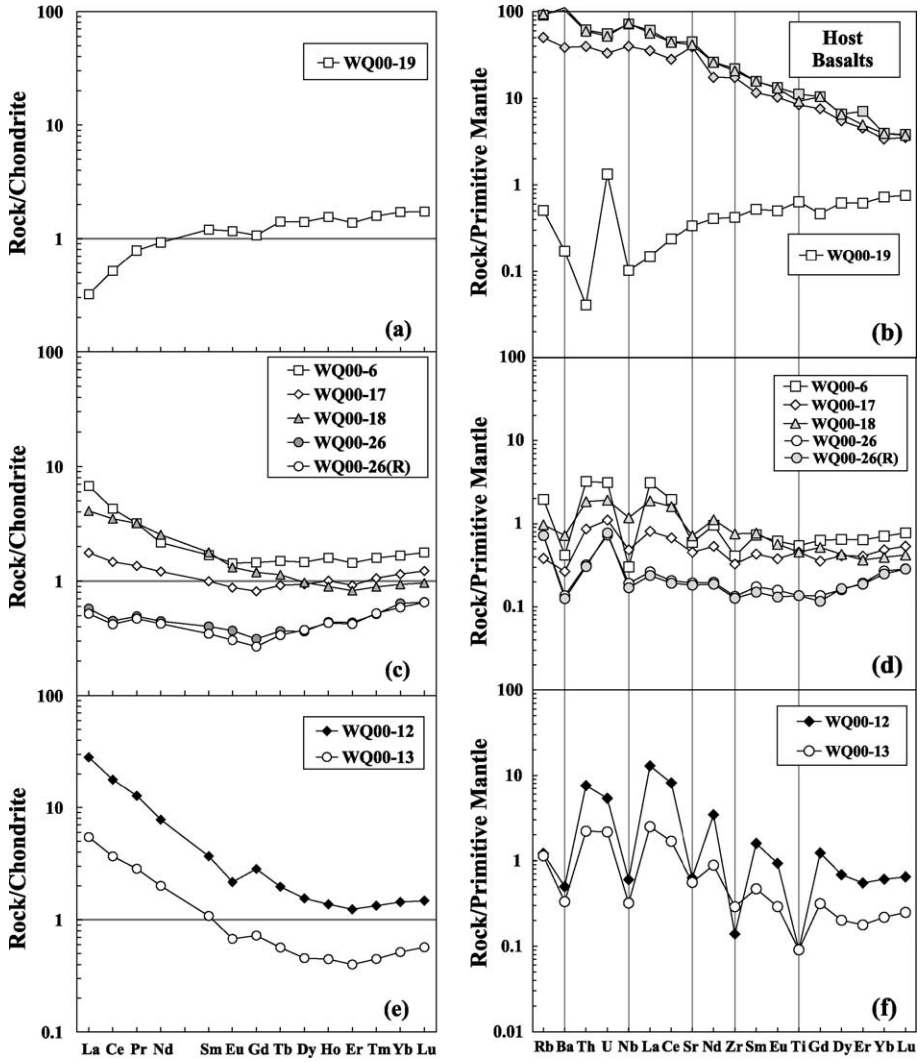

Fig. 7. Chondrite-normalized rare earth element patterns (a,c,e) and primitive mantle-normalized element patterns (b,d,f) for mantle peridotites from Wangqing, NE China. The trace elements are arranged in the order of decreasing incompatibility from left to right. The normalized values are from Sun and McDonough (1989). The peridotites are divided into three groups based on REE pattern type. The data of host basalts are from Liu et al. (1994).

5. Results

5.1. Major and trace element geochemistry

Peridotites from each of the three locales display a wide range of major and trace elemental compositions (Tables 1–3). Samples range from refractory harzburgite to fertile lherzolite (Fig. 3). Most samples lie along the oceanic trend of Boyd (1989), but sample DAL02-2 (wehrlite) from Longgang and BBT1-12 and BBT1-14 from Shuangliao have somewhat higher CaO, which might have resulted from unrepresentative sampling due to the small sample size, or later addition of Ca-rich clinopyroxene. Other than for these three samples, the linear correlation between the Al_2O_3 content of the whole-rocks, and Fo and Cr# values of olivine and spinel, respectively, indicate that bulk-rock Al_2O_3 serves as a viable index of fertility (Table 4; Fig. 4).

Three distinct types of whole-rock REE patterns are identified in each locale (Figs. 5–7): (1) Fertile lherzolites exhibit an LREE-depleted pattern. (2) Less fertile lherzolites are characterized by spoon-shaped REE patterns. Unlike the LREE-depleted patterns, they show an upward inflection in La. (3) LREE-enriched patterns are found in the depleted harzburgite and clinopyroxenite-poor lherzolites. The exceptions are samples DYS0-05 and L-1, which are LREE-depleted, but not fertile with respect to major element concentrations. That the pronounced LREE enrichment is restricted to the cpx-poor mantle xenoliths is typical of peridotite xenoliths worldwide (McDonough and Frey, 1989; Downes, 2001). It should also be noted, however, that the peridotites from Shuangliao and Wangqing have chondrite-normalized heavy REE (HREE) values of about unity (Figs. 6 and 7), whereas some samples from Longgang show much lower abundances of HREE (Fig. 5), potentially indicating that the lithospheric mantle beneath Longgang experienced much higher degrees of melt extraction than in the suites from Shuangliao and Wangqing.

Whole-rock primitive mantle-normalized trace element distributions are shown in Figs. 5–7. The Longgang peridotites show highly irregular variation patterns. Except for sample L-2, most LREE-depleted samples display enrichments of Ba, U, and sometimes Zr and Ti (Fig. 5b). The spoon-shaped REE lherzolites are characterized by enrichment of U (Fig. 5d), which is also observed in the LREE-depleted samples. The harzburgites have complex patterns (Fig. 5f). Sample DAL02-2 shows significant depletions of Th, U and Ti, but sample LQL1-01 displays pronounced enrichments of Ba, Th and U.

In contrast, the LREE-depleted lherzolites from Shuangliao contain lower concentrations of incompatible elements, but with relative enrichments of Rb, Ba, U and Nb (Fig. 6b). The lherzolites with spoon-shaped REE patterns show evidence for depletion of Ba and Nb, but significant enrichment of Sr (Fig. 6d). The harzburgites contain higher concentrations of incompatible elements, with pronounced depletions in Ba, Nb, Zr and Ti (Fig. 6f).

For the Wangqing peridotites, the LREE-depleted lherzolites contain lower concentrations of most incompatible elements, but with relative enrichments of Rb, Ba and U. The lherzolites with spoon-shape REE patterns show depletions of Ba, Nb and for some samples, Sr, Zr and Ti. The harzburgites contain higher abundances of most incompatible elements, and pronounced depletions of Ba, Nb, Sr, Zr and Ti. The REE patterns and elemental plots for these rocks suggest variable extents of melt extraction and metasomatic alteration.

5.2. Re–Os isotopic geochemistry

Osmium and Re concentrations range from 0.11 to 5.10 ppb, and from below detection to 0.42 ppb,

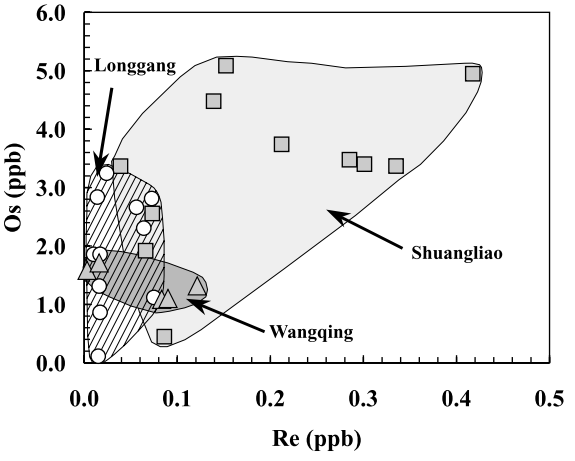

Fig. 8. The Re and Os abundances of studied mantle peridotite xenoliths in NE China. Note the extremely low concentrations of Re in the Longgang samples.

respectively (Table 4). Samples BLS1-09 (Shuangliao) and DYS1-05 (Dayishan, Longgang, hornblende-bearing) have unusually low Os concentrations. Such low concentrations in peridotites have been occasionally noted in other peridotite suites (e.g. Meisel et al., 2001). Most of the Os and Re concentrations for

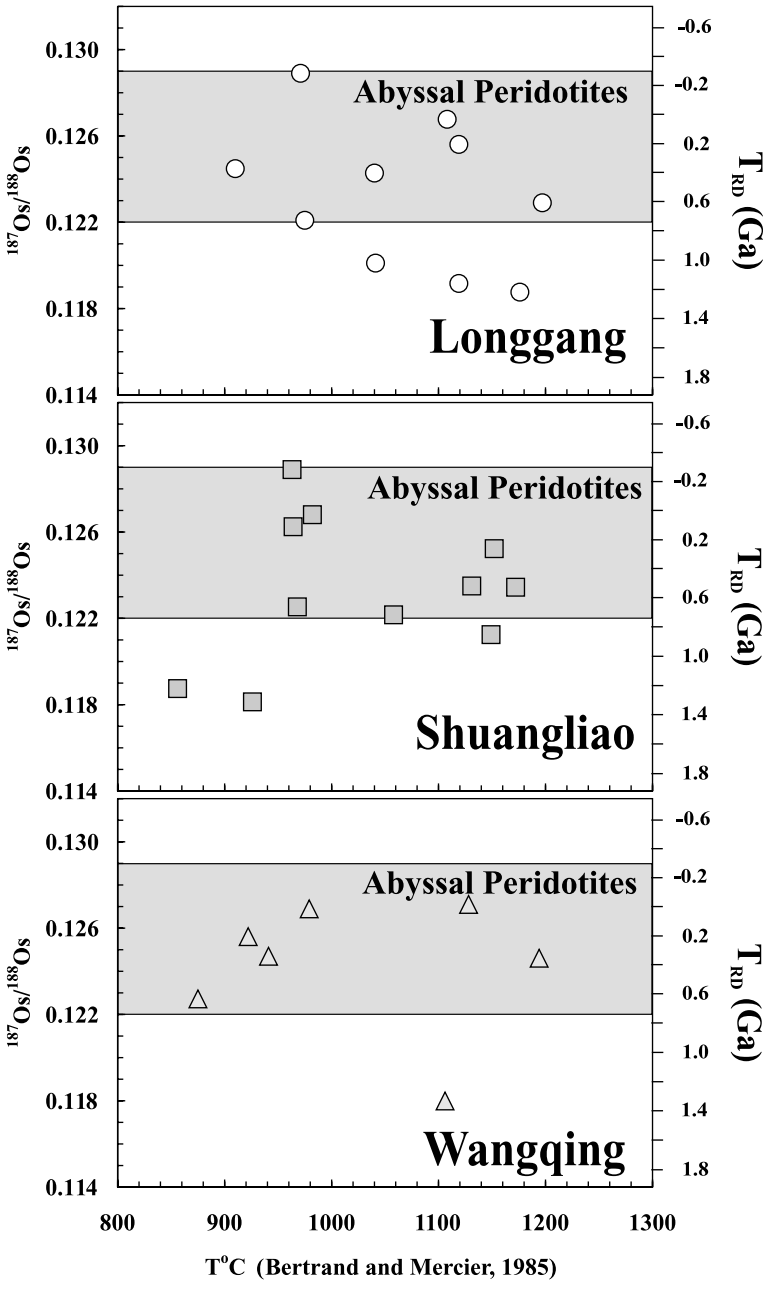

Fig. 9. Plots of equilibrium temperature (two-pyroxene geothermometer of Bertrand and Mercier, 1985) against Os isotopic composition, indicating the complex vertical age structure for different SCLM. The average abyssal peridotites are from Snow and Reisberg (1995).

peridotites, however, are typical of worldwide occurrences of mantle peridotites. Compared with those in Longgang and Wangqing, however, most Shuangliao samples have higher abundances of Re (Fig. 8). This could be the result of Re addition to the Shuangliao samples, or Re loss from the Longgang and Wangqing samples, as a result of surficial weathering. Xenoliths from the three locales have $^{187}Re/^{188}Os$ ratios ranging from <0.01 to 0.926, but most samples are subchondritic, with 23 of 29 samples having ratios <0.4. Moreover, the Longgang samples have $^{187}Re/^{188}Os$ ratios that are much lower, and have a narrower range, than those of the Shuangliao and Wangqing suites. Consequently, all samples have minimal in situ accumulation of ^{187}Os since their removal to the surface. As is common for peridotite xenolith suites from SCLM, the $^{187}Re/^{188}Os$ ratios for samples from the different locales do not correlate with their $^{187}Os/^{188}Os$ ratios. The lack of correlation can be attributed to several factors including the likelihood of derivation of samples from isotopically distinct portions of the SCLM, and the possibility of late-stage Re mobility (e.g. Chesley et al., 1999; Meisel et al., 2001). It is important to note, however, that in all three studied locales, the refractory samples have lower $^{187}Re/^{188}Os$ ratios than those of fertile lherzolites, which suggests that later-stage metasomatic alteration did not result in an increase in Re abundances.

There is no simple correlation between the equilibration temperature, determined by two-pyroxene geothermometry (Bertrand and Mercier, 1985) and the Os isotopic ratio among the studied peridotite samples (Table 4; Fig. 9), as might be expected if there were a correlation between extent of melting and depth. In Longgang, the more depleted and refractory samples show higher temperature equilibration, but in Shuangliao, the two most depleted samples (BLS1-8 and BBT1-8) have lowest equilibration temperatures. In Wangqing, the most depleted sample (WQ00-18) has an intermediate equilibration temperature.

6. Discussion

6.1. Overview of Os model ages

Mantle melting that ultimately leads to the production of continental crust can also generate buoyant subcontinental lithospheric mantle (SCLM) that forms a long-lived keel to continental crust (Jordan, 1988; Boyd, 1989; Walker et al., 1989; Menzies, 1990). Some portions of the SCLM may be subsequently affected by rifting or subduction following cratonization (e.g. Chesley et al., 1999; Lee et al., 2000). These processes may cause the removal of SCLM that was spatially associated with overlying crust, as has been suggested for northeastern China. Ancient SCLM that is in some manner removed from overlying craton would likely be replaced by younger lithospheric mantle derived from the convecting upper mantle, so one mechanism for identifying this type of process is via the identification of significantly younger lithospheric mantle than is consistent with the age of the overlying crust.

Although constraining the formation age of SCLM is difficult because of its high equilibration temperatures and open-system geochemical behaviour, the $^{187}Re–^{187}Os$ isotopic system has proven useful for placing minimum age constraints on the melt depletion events that likely coincide with the formation of SCLM (Walker et al., 1989; Carlson and Irving, 1994; Pearson, 1999a,b; Carlson et al., 2000; Peslier et al., 2000a,b). Partial melting of the mantle, leading to the creation of SCLM and overlying craton, leaves a variably Re-depleted residue that results in retardation in the growth of the $^{187}Os/^{188}Os$ ratio, compared to the generally chondritic evolution of the convecting upper mantle (e.g. Walker et al., 2002). The mantle residue is relatively immune to subsequent resetting because of its high Os content and the removal of the parent element.

Osmium model ages may provide constraints on the timing of melt depletion. For example, T_{MA} model age calculations (Walker et al., 1989; Shirey and Walker, 1998) are based on the extrapolation of the Os isotope composition of a xenolith from the time it is brought to the surface, to the chondritic evolution trajectory, as projected from the current $^{187}Re/^{188}Os$ ratio of the sample. T_{MA} model ages often lead to aberrant values (both future ages and ages older than the Earth), probably resulting from post-melting perturbation of Re during metasomatism or alteration. This is because Re can be quite mobile in peridotite xenoliths, and may be added or removed from a xenolith in transit to the surface from the mantle, or while residing near the surface. Time of Re depletion

(T_{RD}) model ages are more robust indicators of the minimum age of melt depletion (Walker et al., 1989; Pearson et al., 1995a,b). T_{RD} model ages are calculated by assuming that melting removes all of the Re from the peridotite (Walker et al., 1989). T_{RD} ages may approach the true age of melting for very highly refractory peridotites, as Re is almost completely removed from the residue at very high degrees of melting. The T_{RD} ages for highly refractory samples (e.g. $Al_2O_3 < 1.2$ wt.%) probably provide the best constraints on the minimum age of melt depletion for a suite of ultramafic mantle xenoliths. Nonetheless, T_{RD} ages may significantly underestimate a melt depletion event for samples that have experienced only partial Re removal.

An additional complexity in the interpretation of whole-rock Os data for age constraints is evidence for multiple generations of sulfides present in some suites of mantle xenoliths. In situ studies of sulfides within individual peridotites have revealed significant variability in $^{187}Os/^{188}Os$ ratios (e.g. Pearson et al., 2002). This suggests that different Os-rich sulfides were generated at different times, although it remains unclear what the mass balance of the various sulfides populations are within an individual sample. Despite this observation, T_{RD} ages for bulk rocks provide a minimum age constraint for likely the primary melt depletion event.

6.2. Ages of SCLM beneath NE China

As noted above, Gao et al. (2002) reported Archean Os model ages for xenoliths erupted during the early Paleozoic at Fuxian. The two samples examined had $^{187}Os/^{188}Os$ ratios < 0.112. Indeed, data for suites of xenoliths worldwide show that Archean SCLM is dominated by low $^{187}Os/^{188}Os$ ratios of < 0.112 (Pearson, 1999a,b, and references therein). In contrast to xenoliths from Fuxian, xenoliths sampled by the Cenozoic volcanic systems piercing the NCC have much higher $^{187}Os/^{188}Os$ ratios, despite having similarly refractory compositions (Fig. 10). The lowest $^{187}Os/^{188}Os$ ratio of 0.117, reported for a Hannouba xenolith by Gao et al. (2002), is consistent with a T_{RD} model age of 1.5 Ga. (Note that Gao et al. (2002) calculated T_{RD} ages using mantle parameters equivalent to PUM, rather than the convention of the carbonaceous chondrite average. As a consequence, their model ages are approximately 0.3 Ga older than ages calculated using the chondritic parameters. Here we recalculate their data to correspond with our model ages that are based on the carbonaceous chondrite reference.) They also reported an errorchron age of 1.9 ± 0.2 Ga for a selected suite of xenoliths. Hannouba is located approximately 1000 km southwest of Longgang. Four refractory to highly refractory samples from Longgang, L-1, LQL1-13, DYS1-03 and DAL02-2, have T_{RD} ages of 1.0–1.2 Ga, suggesting a minimum Mesoproterozoic model age for melt depletion of the SCLM underlying this portion of the craton. Similarly, Gao et al. (2002) reported a T_{RD} age of 1.0 Ga for one highly refractory xenolith from Qixia, which is located approximately 800 km to the southeast of Longgang. The lack of more refractory samples from these three locales suggests that materials with significantly more depleted Os are not likely to be found, at least within the suites sampled. Consequently, there is no evidence in the three Cenozoic suites of the NCC for the presence of Archean SCLM during the Cenozoic. Instead, the new results, combined with the results from Gao et al. (2002), suggest that at the time of sampling during the Cenozoic, there was instead appreciable Mesoproterozoic SCLM underlying the NCC.

Two highly refractory samples ($Al_2O_3 < 1.2$ wt.%) from Longgang, DAL02-3 and LQL1-01, have much younger T_{RD} ages of 0.6 and 0.4 Ga. Also, the suite of xenoliths from Qixia, studied by Gao et al. (2002), is dominated by T_{RD} ages ranging from 0.4 to 0 Ga, although with the exception of the sample noted above, none of these samples were highly refractory. The younger model ages, particularly for the highly refractory samples from Longgang, suggest that some portions of the SCLM underlying the NCC during the Cenozoic were dominated by lithosphere that experienced extensive melt extraction during the Phanerozoic. Thus, the SCLM underlying the sampled regions of the NCC during the Cenozoic evidently ranges in age from about 1.9 Ga to some time in the Phanerozoic.

Data for the samples from the XMOB also display complicated Os isotopic systematics. For the entire Shuangliao suite, the $^{187}Os/^{188}Os$ ratios range from 0.118 to 0.129, which correspond with model T_{RD} ages that range from 1.3 Ga to future ages (meaning

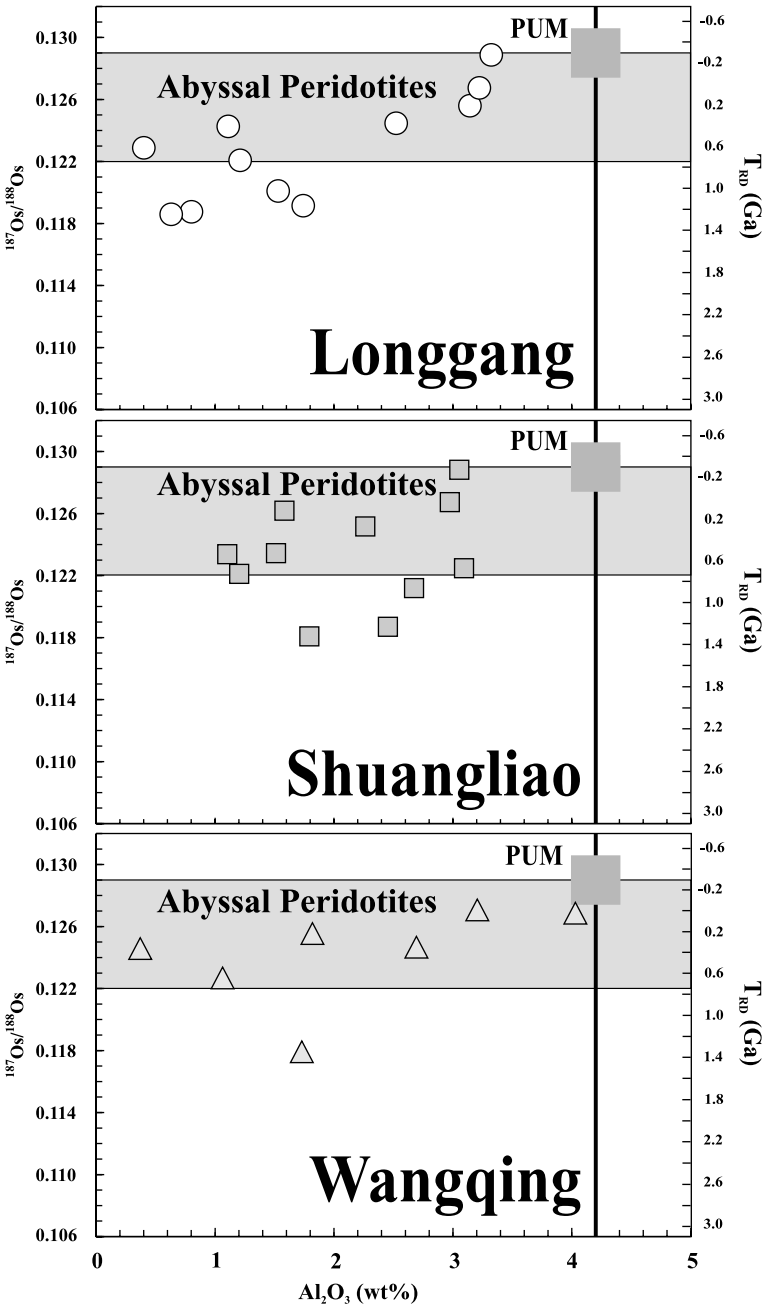

Fig. 10. Os isotopic composition versus Al_2O_3 (wt %). The average abyssal peridotite data are from Snow and Reisberg (1995). PUM—Primitive Upper Mantle (Meisel et al., 2001).

the $^{187}Os/^{188}Os$ of these samples are slightly higher than the modern chondritic average). Three samples (BBT1-08, BLS1-08, WQ00-18) give T_{RD} model ages of 1.2 and 1.3 Ga, respectively, which correspond well with the T_{DM} Nd model ages for the overlying crust (Fig. 2).

As in the NCC suite, some samples within the XMOB indicate a much younger melt depletion event(s). Four of the most refractory samples, BBT1-14 and BBT2-12 from Shuangliao and WQ00-12 and WQ00-13 from Wangqing, yield T_{RD} model ages of 0.7–0.1 Ga. As with the NCC, results for these samples suggest that there were both Mesoproterozoic and Phanerozic additions to the SCLM underlying the XMOB.

6.3. Implications for the tectonic evolution of the SCLM beneath NE China

Our results reveal complexity in the age structure of the SCLM underlying northeastern China. The results from Fuxian (Gao et al., 2002) indicate that thick Archean SCLM underlay at least some portion of the NCC during the early Paleozoic, yet xenoliths that sampled the SCLM beneath the NCC during the Cenozoic do not sample Archean SCLM. Instead, the Cenozoic xenoliths sample SCLM that underwent melt depletion during the Paleo- and Mesoproterozic, and also much later, during the Phanerozoic. Thus, the age relation between the NCC and underlying SCLM is very different from the age relations between most other cratons and their underlying SCLM. Most studies reveal similar ages between SCLM and overlying craton (e.g. Walker et al., 1989; Carlson and Irving, 1994; Pearson, 1999a,b; Carlson et al., 2000; Lee et al., 2001). The new results for the NCC are consistent with the results reported by Gao et al. (2002), and suggest that the complex age structure of the SCLM underlying the NCC extends areally over more than 1000 km. The combined results suggest that Archean SCLM was removed from under the NCC, most likely subsequent to the early Paleozoic. The lithospheric mantle that was removed, evidently was replaced by material with an Os isotopic composition similar to that of the convecting upper mantle at the same time. This lithospheric mantle then became variably melt depleted.

Gao et al. (2002) attributed the removal event to the collision of the Yangtze craton and NCC during the Triassic. In contrast, we suggest that the subduction of the Pacific Oceanic Plate subsequent to the late Mesozoic was the main cause of this lithospheric removal. This interpretation is based on the observation that the Triassic collisional zone between the Yangtze Craton and NCC extended in an E–W direction with no significant sign of the coeval magmatism that would likely be associated with lithospheric removal (Kay and Kay, 1993). The new results for the XMOB indicate that Phanerozoic SCLM also resides beneath this crustal block (far from the collisional zone), and recent studies of the SCLM mantle beneath southeastern and central eastern China have also shown evidence for Phanerozoic additions (Xu et al., 2000, 2002; Zhi et al., 2001). Thus, it appears that Phanerozoic SCLM was added to most parts of eastern China along a NNE trend. This is consistent with the formation of the new lithosphere being related to the evolution of the circum-Pacific continental margin during the late Mesozoic and the Cenozoic. Conclusively discriminating between our model and the model of Gao et al. (2002), however, will not be easy. Osmium isotopes provide no age resolution for Phanerozoic events, and so cannot provide confirming chronologic evidence for a correspondence between the collisional or subduction events, and the lithospheric additions.

Based on the Proterozoic model ages for samples from Hannouba, Gao et al. (2002) also concluded that some portion of the original Archean SCLM underlying the NCC was removed during the Proterozic, and replaced with new lithosphere derived from the convecting upper mantle. However, it is not clear whether the Paleo- to Meso-Proterozoic SCLM sampled at Hannouba, Longgang, and to a lesser extent at Qixia and Wangqing, was juxtaposed beneath the NCC at the time of the purported subduction, or was present prior to the early Paleozoic. The limited data for the early Paleozoic SCLM from Fuxian reveal no Proterozoic lithosphere, but only two samples have yet been analyzed. One highly refractory sample from the Ordovician Mengyin kimberlites, in contrast, gives a T_{RD} age of 0.7 Ga (Gao et al., 2002). The Os isotopic results for the SCLM underlying the XMOB are quite similar to those of the NCC, despite the major difference in age between the two cratonic blocks. Indeed, the trace element characteristics of xenoliths from the SCLM underlying both blocks are also generally similar. Unlike for the NCC, there is a general concordance of model ages between some portions of the SCLM and the overlying crust in the XMOB (during the Cenozoic sampling), although most Nd model ages for the crustal rocks are somewhat younger than the Os model ages for the SCLM (0.9 vs. 1.2 Ga). As with the NCC

samples, there are also samples with compositions consistent with Phanerozoic additions to the lithospheric mantle from the convecting upper mantle. These additions may also be related to subduction of the Pacific plate since the late Mesozoic. Whatever processes caused the range in lithospheric ages, they did not evidently result in the production of a keel that is stratified with regard to age versus depth (e.g. Fig. 9), and may indicate that the Proterozoic and Phanerozoic SCLM is complexly intermixed under northeastern China.

7. Conclusions

The combined results of this and previous studies confirm that tectonic activities can severely disrupt the synchronous age structure between mantle lithospheric keels and overlying cratonic crust. In northeastern China, two cratonic blocks, the NCC and the XMOB, with crustal residence ages of about 2500–2800 and 600–1000 Ma, respectively, overlie SCLM with both Proterozoic and Phanerozoic model ages. In the NCC, the Proterozoic SCLM is much younger than the overlying Archean crust, suggesting that crust–mantle decoupling may have occurred during the Proterozoic, the Phanerozoic, or during both periods. In contrast, the age of some portions of the SCLM underlying the XMOB are generally comparable to that of the crust. The young new lithospheric mantle, derived from the convecting upper mantle, was evidently added to both cratonic blocks during the Phanerozoic. This lithopheric mantle removal and replenishment likely has led to the thinning of the lithosphere during the Phanerozoic as suggested via geophysical and petrologic studies.

Acknowledgements

This work was supported by grants (40133020, 49872031) from the National Natural Science Foundation of China (to F.-Y.W) and National Science Foundation Grant EAR 9909197 (to RJW). Fu-yuan Wu acknowledges the hospitality of the *Isotope Geochemistry Laboratory* during his visits to Maryland (May of 2000 and February–March of 2002). A. Gangopadhyay, H. Becker and P. Tomascak are thanked for their help during the chemical separation and mass spectrometric analyses. Reviews of early drafts by R.L. Rudnick substantially improved this manuscript. Constructive reviews by A.H. Peslier and C.-T. Lee have substantially improved the final draft. **[RR]**

References

Basu, A.R., Wang, J.-W., Huang, W.-K., Xie, G.-H., Tatsumoto, M., 1991. Major element, REE, and Pb, Nd and Sr isotopic geochemistry of Cenozoic volcanic rocks of eastern China: implications for their origin from suboceanic-type mantle reservoirs. Earth Planet. Sci. Lett. 105, 149–169.

Bertrand, P., Mercier, J.-C., 1985. The mutual solubility of coexisting ortho- and clinopyroxene: toward an absolute geothermometer for the natural system? Earth Planet. Sci. Lett. 76, 109–122.

Boyd, F.R., 1989. Compositional distinction between oceanic and cratonic lithosphere. Earth Planet. Sci. Lett. 96, 15–26.

Carlson, R.W., Irving, A.J., 1994. Depletion and enrichment history of subcontinental lithospheric mantle: an Os, Sr, Nd and Pb isotopic study of ultramafic xenoliths from the northwestern Wyoming Craton. Earth Planet. Sci. Lett. 126, 457–472.

Carlson, R.W., Boyd, F.R., Shirey, S.B., et al., 2000. Continental growth, preservation, and modification in Southern Africa. GSA Today 10 (2), 1–7.

Chesley, J.T., Rudnick, R.L., Lee, C.-T., 1999. Re–Os systematics of mantle xenoliths from the east African rift: age, structure, and history of the Tanzanian craton. Geochim. Cosmochim. Acta 63, 1203–1217.

Chi, J.-S. (Ed.), 1988. The Study of Cenozoic Basalts and Upper Mantle Beneath Eastern China. China University of Geosciences Publishing House, Wuhan.

Cohen, A.S., Waters, F.G., 1996. Separation of osmium from geological materials by solvent extraction for analysis by TIMS. Anal. Chim. Acta 332, 269–275.

Downes, H., 2001. Formation and modification of the shallow subcontinental lithospheric mantle: a review of geochemical evidence from ultramafic xenolith suites and tectonically emplaced ultramafic massifs of Western and Central Europe. J. Petrol. 42, 233–250.

E, M.-L., Zhao, D.-S. (Eds.), 1987. Cenozoic Basalts and Deep-Seated Rock Xenoliths in Eastern China. Science Press, Beijing.

Fan, Q.-C., Hooper, P.R., 1989. The mineral chemistry of ultramafic xenoliths of eastern China: implications for upper mantle composition and the paleogeotherms. J. Petrol. 30, 1117–1158.

Fan, W.-M., Zhang, H.-F., Baker, J., Jarvis, K.E., Mason, P.R.D., Menzies, M.A., 2000. On and off the North China Craton: where is the Archean keel? J. Petrol. 41, 933–950.

Gao, S., Rudnick, R.L., Carlson, R.W., McDonough, W.F., Liu, Y.-S., 2002. Re–Os evidence for replacement of ancient mantle lithosphere beneath the North China Craton. Earth Planet. Sci. Lett. 198, 307–322.

Griffin, W.L., Zhang, A.-D., O'Reilly, S.Y., Ryan, C.G., 1998. Pha-

nerozoic evolution of the lithosphere beneath the Sino-Korean craton. In: Flower, M.F.J., Chung, S.-L., Lo, C.-H., Lee, T.-Y. (Eds.), Mantle Dynamics and Plate Interactions in East Asia. Geodyn. Ser., vol. 27. Am. Geophy. Union, Washington, DC, pp. 107–126.

Hu, S.-H., Chen, A.-F., Lin, S.-L., Yuan, H.-L., Gao, S., 2000. ICP-MS analytical research into 40 trace and ultra-trace elements in geological samples (in Chinese with English abstract). Earth Sci. 25, 186–190.

Jahn, B.-M., Wu, F.-Y., Chen, B., 2000. Massive granitoids generation in Central Asia: Nd isotope evidence and implication for continental growth in the Phanerozoic. Episodes 23, 82–92.

Jordan, T.H., 1988. Structure and formation of the continental tectosphere. J. Petrol., Special Lithosphere Issue, 11–37.

Kay, R.W., Kay, S.M., 1993. Delamination and delamination magmatism. Tectonophysics 219, 177–189.

Lee, C.-T., Yin, Q.-Z., Rudnick, R.L., Chesley, J.T., Jacobsen, S.B., 2000. Osmium isotopic evidence for Mesozoic removal of lithospheric mantle beneath the Sierra Nevada, California. Science 289, 1912–1916.

Lee, C.-T., Yin, Q.-Z., Rudnick, R.L., Jacobsen, S.B., 2001. Preservation of ancient and fertile lithospheric mantle beneath the southwestern United States. Nature 411, 69–73.

Liu, R.-X. (Ed.), 1992. The Age and Geochemistry of Cenozoic Volcanic Rocks in China. Seismic Press, Beijing.

Liu, J.-Q., 1999. Active Volcanoes in China (in Chinese). Science Press, Beijing.

Liu, D.-Y., Nutman, A.P., Compston, W., Wu, J.-S., Shen, Q.-H., 1992. Remmants of $\geq$3800 Ma crust in the Chinese part of the Sino-Korean Craton. Geology 20, 339–342.

Liu, C.-Q., Masuda, A., Xie, G., 1994. Major- and trace-element compositions of Cenozoic basalts in eastern China: petrogenesis and mantle source. Chem. Geol. 114, 19–42.

McDonough, W.F., Frey, F.A., 1989. Rare-earth elements in upper mantle rocks. In: Lipin, B.R., McKay, G.A. (Eds.), Geochemistry and Mineralogy of Rare Earth Elements. Mineral. Soc. Am. Rev. Miner., vol. 21, pp. 99–145.

Meisel, T., Walker, R.J., Irving, A.J., Lorand, J.-P., 2001. Osmium isotopic compositions of mantle xenoliths: a global perspective. Geochim. Cosmochim. Acta 65, 1311–1323.

Menzies, M.A., 1990. Archean, Proterozoic, and Phanerozoic lithosphere. In: Menzies, M.A. (Ed.), Continental Mantle. Oxford Univ. Press, New York, pp. 67–86.

Menzies, M.A., Xu, Y.-G., 1998. Geodynamics of the North China Craton. In: Flower, M.F.J., Chung, S.-L., Lo, C.-H., Lee, T.-Y. (Eds.), Mantle Dynamics and Plate Interactions in East Asia. Geodyn. Ser., vol. 27. Am. Geophy. Union, Washington, DC, pp. 155–165.

Menzies, M.A., Fan, W.-M., Zhang, M., 1993. Palaeozoic and Cenozoic lithoprobe and the loss of >120 km of Archean lithosphere, Sino-Korean craton, China. In: Prichard, H.M., Alabaster, T., Harris, N.B.W., Neary, C.R. (Eds.), Magmatic Processes and Plate Tectonics. Geol. Soc. Spec. Publ., vol. 76, pp. 71–81.

Pearson, D.G., 1999a. The age of continental roots. Lithos 48, 171–194.

Pearson, D.G., 1999b. Evolution of cratonic lithospheric mantle: an isotopic perspective. In: Fei, Y., Bettka, C.M., Mysen, B.O. (Eds.), Mantle Petrology: Field Observations and High Pressure Experimentation. Geochem. Soc. Spec. Publ., vol. 6, pp. 57–78.

Pearson, D.G., Shirey, S.B., Carlson, R.W., Boyd, F.R., Pokhilenko, N.P., Shimizu, N., 1995a. Re–Os, Sm–Nd and Rb–Sr isotope evidence for thick Archean lithospheric mantle beneath the Siberia craton modified by multi-stage metasomatism. Geochim. Cosmochim. Acta 59, 959–977.

Pearson, D.G., Shirey, S.B., Carlson, R.W., Boyd, F.R., Nixon, P.H., 1995b. Stabilisation of Archean lithospheric mantle: a Re–Os isotope study of peridotite xenoliths from the Kaapvaal craton. Earth Planet. Sci. Lett. 134, 341–357.

Pearson, N.J., Alard, O., Griffin, W.L., Jackson, S.E., O'Reilly, S.Y., 2002. In situ measement of Re–Os isotopes in mantle sulfides by laser ablation multicollector-inductively coupled plasma mass spectrometry: analytical methods and preliminary results. Geochim. Cosmochim. Acta 66, 1037–1050.

Peng, Z.-C., Zartman, R.F., Futa, K., Chen, D.-G., 1986. Pb-, Sr-, and Nd-isotopic systematics and chemical characteristics of Cenozoic basalts, eastern China. Chem. Geol. 59, 3–33.

Peslier, A.H., Reisberg, L., Ludden, J., Francis, D., 2000a. Os isotopic systematics in mantle xenoliths; age constraints on the Canadian Cordillera lithosphere. Chem. Geol. 166, 85–101.

Peslier, A.H., Reisberg, L., Ludden, J., Francis, D., 2000b. Re–Os constraints on harzburgite and lherzolite formation in the lithospheric mantle: a study of northern Canadian Cordillera xenoliths. Geochim. Cosmochim. Acta 64, 3061–3071.

Qi, Q., Taylor, L.A., Zhou, X.-M., 1995. Petrology and geochemistry of mantle peridotite xenoliths from southeastern China. J. Petrol. 36, 55–79.

Shirey, S.B., Walker, R.J., 1995. Carius tube digestions for low-blank rhenium–osmium analysis. Anal. Chem. 67, 2136–2141.

Shirey, S.B., Walker, R.J., 1998. The Re–Os isotope system in cosmochemistry and high temperature geochemistry. Annu. Rev. Earth Planet. Sci. 26, 423–500.

Snow, J.E., Reisberg, L., 1995. Os isotopic systematics of the MORB mantle: results from altered abyssal peridotites. Earth Planet. Sci. Lett. 136, 723–733.

Snyder, G.A., Taylor, L.A., Jin, Y.-Q., Taylor, D.-H., 1997. Mantle-lherzolite xenoliths from eastern China: petrogenesis and development of secondary textures. Int. Geol. Rev. 39, 671–687.

Sun, S.-S., McDonough, W.F., 1989. Chemical and isotopic systematics of oceanic basalts: implications for mantle composition and processes. In: Saunders, A.D., Norry, M.J. (Eds.), Magmatism in the Ocean Basins. Geol. Soc. Spec. Publ., vol. 42, pp. 313–345.

Tatsumoto, M., Basu, A.R., Huang, W.-K., Wang, J.-W., Xie, G.-H., 1992. Sr, Nd, and Pb isotopes of ultramafic xenoliths in volcanic rocks of Eastern China: enriched components EMI and EMII in subcontinental lithosphere. Earth Planet. Sci. Lett. 113, 107–128.

Walker, R.J., Carlson, R.W., Shirey, S.B., Boyd, F.R., 1989. Os, Sr, Nd, and Pb isotope systematics of southern African peridotite xenoliths: implications for the chemical evolution of subcontinental mantle. Geochim. Cosmochim. Acta 53, 1583–1595.

Walker, R.J., Morgan, J.W., Horan, M.F., Czamanske, G.K., Krogstad, E.J., Fedorenko, V.A., Kunilov, V.E., 1994. Re–Os isotopic evidence for an enriched-mantle source for the Noril'sk-type, ore-bearing intrusions, Siberia. Geochim. Cosmochim. Acta 58, 4179–4197.

Walker, R.J., Prichard, H.M., Ishiwatari, A., Pimentel, M., 2002. The osmium isotopic composition of convecting upper mantle deduced from ophiolite chromites. Geochim. Cosmochim. Acta 66, 329–345.

Wang, H.-Z., Mo, X.-X., 1996. An outline of the tectonic evolution of China. Episodes 18, 6–16.

Wang, W.-Y., Takahashi, E., Sueno, S., 1998. Geochemical properties of lithospheric mantle beneath the Sino-Korea craton; evidence from garnet xenocrysts and diamond inclusions. Phys. Earth Planet. Inter. 107, 249–260.

Wu, F.-Y., Ge, W.-C., Sun, D.-Y., Zhou, Y., 1997. The Sm–Nd, Rb–Sr isotopic ages of the Archean granites in southern Jilin Province (in Chinese with English abstract). Acta Petrol. Sin. 13, 499–506.

Wu, F.-Y., Jahn, B.-M., Wilde, S.A., Sun, D.-Y., 2000. Phanerozoic continental crustal growth: U–Pb and Sr–Nd isotopic evidence from the granites in northeastern China. Tectonophysics 328, 89–113.

Wu, F.-Y., Sun, D.-Y., Li, H.-M., Jahn, B.-M., Wilde, S.A., 2002. A-type granites in Northeastern China: age and geochemical constraints on their petrogenesis. Chem. Geol. 187, 143–173.

Wu, F.-Y., Zhao, G.-C., Wilde, S.A., Sun, D.-Y., 2003. Nd isotopic constraints on the crustal formation of the North China Craton. J. Asian Earth Sci. (in press).

Xu, Y.-G., Ross, J.V., Mercier, J.-C.C., 1993. The upper mantle beneath the continental rift of Tanlu, Eastern China: evidence for the intralithospheric shear zones. Tectonophysics 225, 337–360.

Xu, Y.-G., Menzies, M.A., Vroon, P., Mercier, J.-C., Lin, C.-Y., 1998. Texture–temperature–geochemistry relationships in the upper mantle as revealed from spinel peridotite xenoliths from Wangqing, NE China. J. Petrol. 39, 469–493.

Xu, X.-S., O'Reilly, S.Y., Griffin, W.L., Zhou, X.-M., 2000. Genesis of young lithospheric mantle in Southeastern China: an LAM-ICPMS trace element study. J. Petrol. 41, 111–148.

Xu, Y.-G., Sun, M., Yan, W., Liu, Y., Huang, X.-L., Chen, X.-M., 2002. Xenolith evidence for polybaric melting and stratification of the upper mantle beneath south China. J. Asian Earth Sci. 20, 937–954.

Yu, Y., 1987. Petrology and petrogenesis of the Cenozoic basaltic rocks from Mt. Qixingshan, Jilin Province (in Chinese with English abstract). Acta Petrol. Sin. 3, 55–62.

Zhang, M., Suddaby, P., Thompson, R.N., Thirlwall, M.F., Menzies, M.A., 1995. Potassic volcanic rocks in NE China: geochemical constraints on mantle source and magma genesis. J. Petrol. 36, 1275–1303.

Zhang, M., Suddaby, P., O'Reilly, S.Y., Norman, M., Qiu, J.-S., 2000. Nature of the lithospheric mantle beneath the eastern part of the Central Asian fold belt: mantle xenoliths evidence. Tectonophysics 328, 131–156.

Zheng, J.-P., O'Reilly, S.Y., Griffin, W.L., Lu, F.-X., Zhang, M., 1998. Nature and evolution of Cenozoic lithospheric mantle beneath Shandong Peninsula, Sino-Korean Craton, Eastern China. Int. Geol. Rev. 40, 471–499.

Zheng, J.-P., O'Reilly, S.Y., Griffin, W.L., Lu, F.-X., Zhang, M., Pearson, N.J., 2001. Relict refractory mantle beneath the eastern North China block: significance for lithosphere evolution. Lithos 57, 43–66.

Zhi, X.-C., Peng, Z.-C., Chen, D.-G., Yu, C.-J., Sun, W.-D., Reisberg, L., 2001. The longevity of subcontinental lithospheric mantle beneath Jiangsu–Anhui region. Sci. China, Ser. D 44, 1110–1118.

Zhou, X.-H., Armstrong, R.L., 1982. Cenozoic volcanic rocks of eastern China—secular and geographic trend in chemistry and strontium isotopic composition. Earth Planet. Sci. Lett. 58, 301–329.

Zhou, X.-H., Zhu, B.-Q., Liu, R.-X., Chen, W.-J., 1988. Cenozoic basaltic rocks in eastern China. In: MacDougall, J.D. (Ed.), Continental Flood Basalt. Kluwer, Dordrecht, pp. 311–330.